

One-Electron Interpretation of Optical Absorption and Soft-X-Ray Data in MgO[†]

P. F. Walch

Physics Department, Lewis University, Lockport, Illinois 60441

D. E. Ellis*

Physics Department, Northwestern University, Evanston, Illinois 60201

(Received 23 April 1973; revised manuscript received 16 August 1973)

The electronic structure of magnesium oxide is investigated, using *both* molecular-cluster and energy-band representations within the Hartree-Fock-Slater scheme. Predictions of the simple one-electron model are correlated with x-ray data; some previous controversies are resolved and additional features explained. The results also suggest that the prominent optical-absorption peak at 10.8 eV may be due to an intraband exciton previously identified in alkali-halide and rare-gas crystal spectra.

I. INTRODUCTION

Magnesium oxide is the lightest of the IIA-VIA compounds which are characterized as cubic ionic materials. These compounds are divalent counterparts of the alkali halides and find extensive use as host materials for studying optical and magnetic properties of a variety of impurities, vacancies, defects, etc. The high strength, high melting temperature, and excellent ir and optical transmission of MgO give rise to numerous technical applications. The fundamental electronic properties of MgO have been the subject of many experiments involving such techniques as optical absorption and reflectivity,¹⁻⁵ soft-x-ray emission and absorption,⁶⁻¹⁰ and electron spectroscopy (ESCA).¹¹⁻¹⁴

Since these experimental techniques are now capable of high accuracy, the results provide an opportunity to develop a better theoretical understanding of electronic states in MgO and related compounds. We shall be interested in comparing predictions of a simple one-electron Hartree-Fock-Slater (HFS) model with experimental data and with previous theoretical efforts. Previous interpretations of x-ray data attempted by Fischer¹⁵ and by Fomichev *et al.*⁸ were based on an ionic band-structure model of the crystal while Dodd and Glenn⁹ have used an empirical molecular-orbital (MO) approach. In this paper HFS results are presented for *both* energy-band and MO models, which resolve some of the earlier controversies over level assignments and explain additional features of the x-ray data.

Very extensive optical data for MgO are available, much aimed toward understanding the band-edge excitons. Here we consider contributions of the ordinary *one-electron* direct transitions in the energy range 0-20 eV, which can be compared with data of Roessler and Walker,³ and with results of the empirical pseudopotential method (EPM) of Cohen and co-workers.^{4,16} The results suggest that the prominent absorption peak at 10.8 eV may

be due to an intraband (*L* point ?) exciton previously identified in alkali-halide and rare-gas crystal spectra, rather than a one-electron interband transition.

The remainder of the paper is arranged as follows: In Sec. II we discuss the HFS scheme and the implications of localized versus itinerant models for ionic crystals; the computational methods used are presented in Sec. III. Molecular-orbital and energy-band results are presented in Secs. IV and V, respectively. An interpretation of soft-x-ray data is given and comparisons with previous work are made in Sec. VI. The optical absorption is discussed in Sec. VII, and conclusions are drawn in VIII.

II. THEORETICAL MODELS

The relative merits of itinerant versus localized one-electron descriptions of ionic crystals remain unsettled despite many investigations on the subject. These investigations have, until recently, been hampered by a lack of quantitative methods which can provide definite comparisons with experimental data and by difficulties in estimating many-body (correlation) corrections to the one-electron predictions. The gradual development of powerful numerical techniques and the availability of high-resolution data, e.g., soft-x-ray emission and absorption and optical reflectance, provide an opportunity for making more rigorous tests of theoretical models.

From the itinerant point of view, we may mention the augmented-plane-wave (APW) energy-band calculations of DeCicco on KCl,¹⁷ which show that ground-state properties such as cohesive energy can be obtained to good accuracy. On the other hand, the extensive APW work of Mattheiss on the transition-metal monoxides¹⁸ leads to the conclusion that a band representation may be inadequate for transport and other excited-state properties. A localized-orbital picture has been put forward,

for example, in the studies of Kunz,¹⁹ Lipari,²⁰ and others on the alkali-halide and rare-gas crystals, where in particular one-electron binding energies are examined.

In this work we explore the predictions of a (non-self-consistent) HFS model for the occupied levels and low-energy excitations of MgO, adopting the simplest one-electron direct-transition interpretation of the excitation spectrum. Thus the effective Hamiltonian is

$$H = T + V_c + V_x, \quad (1)$$

where the first two terms are the kinetic energy and Coulomb potential, respectively, and the exchange operator V_x is approximated by the local potential

$$V_x = -3\alpha (3\rho/8\pi)^{1/3}. \quad (2)$$

(Hartree atomic units are used unless otherwise specified.) Here the exchange coefficient α is treated as an adjustable parameter, $\frac{2}{3} \leq \alpha \leq 1$, selected to match some feature of the experimental data, although various theoretical prescriptions have been proposed.²¹⁻²⁴ In our non-self-consistent-field (non-SCF) approach the crystal charge density ρ is approximated by the superposition of atomic (ionic) densities as

$$\rho = \sum_{\nu} \rho_{\nu}$$

and the Hamiltonian is thus determined. It is important to note that the full crystal potentials are determined, without making the usual muffin-tin averaging approximations; thus all aspherical "crystal-field" terms are retained.

A single-particle excitation energy can be generally written

$$\Delta E_{i \rightarrow j} = \mathcal{E}_j - \mathcal{E}_i + U_{ij}, \quad (3)$$

where \mathcal{E}_i and \mathcal{E}_j are one-electron eigenvalues of H , and U_{ij} contains self-energy and correlation terms obtained from some many-electron theory. In the Hartree-Fock single determinant model U_{ij} takes a simple well-known form,²⁵ but can be computationally difficult. Further, \mathcal{E}_i and \mathcal{E}_j need not be eigenvalues of the same (ground-state) Hamiltonian, leading to further complications. The "transition state" scheme has been suggested²⁶ as a simple alternative, but requires a separate calculation for each transition. For the present we investigate the simple scheme, generally used in band theory, of determining all \mathcal{E}_i from a single potential and neglecting all U_{ij} corrections.

By comparing the results of a form of localized-orbital (molecular-cluster) calculation with predictions of the Bloch-wave (energy-band) scheme we examine consequences of assumptions about the spatial character of HFS single-particle eigenstates. A reasonably consistent picture is obtained between

molecular-cluster and energy-band predictions, and the experimental data. Significant differences remaining between the simplified HFS model and experiment, which *cannot* be removed merely by exchange scaling provide a measure of "correlation effects" (and possibly self-consistent relaxation effects) in rough accord with estimates in the literature.

III. COMPUTATIONAL METHOD

Approximate eigenvalues and eigenfunctions of the HFS Hamiltonian are generated by means of a discrete variational method (DVM) which has previously been applied to a number of molecular²⁷ and energy-band²⁸ problems. These calculations, and the earlier DVM computations on molecular^{29,30} and nuclear problems³¹ all have in common the selection of a discrete set of sample points in coordinate space, definition of an error functional connected with the Schrödinger equation, and minimization of the error functional over the discrete grid of sample points by a variational procedure. These direct numerical-variational methods have been shown capable of high accuracy in treating potentials of very general form. Details of our formulation of the DVM have been given elsewhere^{32,33}; a brief summary of the approach follows.

The approximate wave functions are expanded in some fixed basis set,

$$\Psi_i(\mathbf{k}, \vec{r}) = \sum_j \chi_j(\mathbf{k}, \vec{r}) C_{ji}(\mathbf{k}), \quad (4)$$

where the basis functions $\chi_j(\mathbf{k}, \vec{r})$ are either (a) symmetry-adapted molecular orbitals belonging to the \mathbf{k} th irreducible representation (irrep) of the molecular-cluster point group, or (b) Bloch orbitals of wave vector \mathbf{k} , belonging to the \mathbf{k} th irrep of the crystal translation group. For all results reported here the basis orbitals were in turn constructed from linear combinations of Slater-type orbitals (STO's) centered at nuclear sites. Gaussian functions, plane waves, and Korringa-Kohn-Rostoker KKR-muffin-tin orbitals³⁴ have been used in other work, as the choice of functions is a matter of convenience.

We define the error functional for state i at point \vec{r} as

$$\delta_i(\vec{r}) = (H - \mathcal{E}_i)\Psi_i(\vec{r}) \quad (5)$$

and minimize the expectation values $\langle \chi_j | \delta_i \rangle$ over some grid of sample points $\{\vec{r}_p\}$, obtaining the matrix secular equation

$$\mathbf{HC} = \mathbf{SCE} \quad (6)$$

for determining the variational coefficients $C_{ij}(\mathbf{k})$. These equations are identical to the conventional Rayleigh-Ritz equations, except that the matrix el-

ements are given as a sample mean, e.g.,

$$H_{ij} = \sum_p w(\vec{r}_p) \chi_i^*(\vec{r}_p) H \chi_j(\vec{r}_p). \quad (7)$$

Here $w(\vec{r})$ is a weight function, generally chosen so that matrix elements converge to their integral values as the number of sample points is increased. Reasonable choices of weight function and distribution of sample points lead to rapid convergence to the Rayleigh-Ritz eigenvalues.

IV. MOLECULAR-CLUSTER RESULTS

Now we may present results for the particular case of the MgO_6 cluster embedded in the magnesium oxide crystal obtained within the HFS-DVM scheme described in the preceding sections. The magnesium atom was placed at the center of the cluster, surrounded by six oxygen atoms in an octahedral configuration. The MgO bond length was taken to be 3.98 a.u.³⁵ in all calculations. The STO basis functions used to expand the molecular orbitals are listed in Table I, and comprise a basis of roughly "double ζ "³⁶ quality. Convergence in energy to 0.01 a.u. in valence and the first few excited energy levels was achieved with the use of 1200 sample points; further convergence was demonstrated with larger numbers of points.³⁷

The input charge densities and atomic Coulomb potentials were computed from the accurate HF atomic orbitals of Clementi.³⁸ Most of the cluster computations were performed with potentials derived from atomic charge densities. This may seem peculiar in view of the common assumption that Mg^{++} and O^{--} ions make up MgO , but the basic one-electron results are rather insensitive to the choice of potential. We must emphasize that this result follows only when the complete potential of the electrically neutral atomic (ionic) crystal is employed; i.e., the external molecular field or crystal-field terms play an important role in determining relative level spacings. However, as was found by successively treating the potentials generated by Mg^0O^0 neutral atom configurations, and Mg^+O^- , and $\text{Mg}^{++}\text{O}^{--}$ ionic configurations, the net effect of assumed ionicity (including distortions

TABLE I. STO basis functions for MgO cluster and energy bands.

Site	Magnesium	Site	Oxygen
nl	ζ	nl	ζ
1s	13.5	1s	10.0
1s	7.5	1s	5.5
2s, p	5.0	2s, p	5.0
2s, p	2.8	2s, p	2.8
3s, p, d	1.9	3s, p	1.9
4s	1.9	3d	1.9 ^a

^aOnly used in band calculation.

TABLE II. Energy levels for MgO_6 cluster, obtained with crystal potential of neutral atom configuration and exchange parameter $\alpha = 0.82$. Results for 1200 sample points (Hartree a.u.).

Irrep:	a_{1g}	e_g	t_{1g}	t_{1u}
	-46.67	-20.02	-0.62	-20.02
	-20.07	-1.20	+0.65 ^a	-1.95
	-3.15	-0.76		-1.20
	-1.22	+0.00 ^a		-0.77
	-0.79	+0.51 ^a		-0.64
	-0.19 ^a			-0.03 ^a
	-0.03 ^a	t_{2g}	t_{2u}	+0.13 ^a
		-0.66	-0.63	+0.54 ^a
		+0.29 ^a	+0.52 ^a	

^aUnoccupied levels.

of the input charge density) is to shift the entire complex of valence and excited-state levels almost uniformly. These results are reproduced in the energy-band calculations discussed in the sequel, and give an indication of the small changes to be expected in proceeding to more complex SCF calculations.

A representative set of one-electron energies is found in Table II, obtained with neutral atom input configurations, and using the optimized exchange scaling parameter $\alpha = 0.82$ (cf. Sec. V). A series of computations were made to study the effects of varying the exchange parameter α , using values ranging from $\frac{2}{3}$ to 1. Since both cluster and band results show the same behavior, a discussion of this feature is postponed until Sec. V. Contributions to the molecular potential from atoms outside the cluster are shown in Fig. 1. The importance of treating this molecular field properly was studied and shifts in MO valence levels of ~ 5 eV were found upon omitting these terms. Much larger shifts were observed for excited-state levels.

Our application of the HFS cluster model to MgO is somewhat artificial, in the sense that no such molecule or complex exists separate from the crystal. Of course, the nearest-neighbor oxygen atoms have the greatest perturbing effect on the central Mg atom, but the 12 next-nearest-neighbor Mg atoms (at $R = 5.61$ a.u.) are arbitrarily excluded from the cluster. Thus the MO wave functions, even when computed under the perturbing influence of the external crystal field, are "valid" only for the cluster. More elaborate calculations, including the orthogonality constraints among localized crystal orbitals, would be desirable; however, it appears that a great deal of experimentally significant information is already available at this level of effort. For example, we compare the molecular-cluster results with those of our energy-band calculations in Fig. 2. The most noteworthy feature

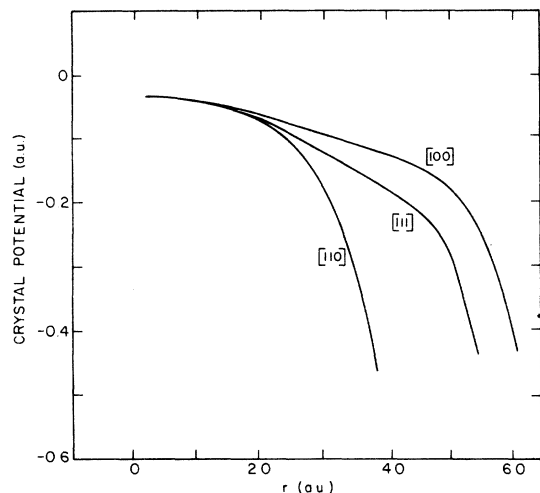


FIG. 1. MgO crystal potential (neutral atom configuration) with central MgO_6 cluster removed.

of this diagram is the cluster of bonding π and σ levels lying between -0.6 and -0.8 a.u. These valence level MO's are predominantly made up of ligand (oxygen) $2p$ character and are separated from the first unoccupied ($6a_{1g}$) MO by an energy gap of roughly 12 eV. The interpretation of MO levels as marking the approximate "center of gravity" of a crystal energy band is seen to be justified. Note in particular the position of the $6a_{1g}$ excited-state level relative to the first conduction band. Since the same Hamiltonian has been employed for both cluster and band calculations, no shifts of the zero of energy are required to achieve this correspondence. The total width of the MO valence band is about 5 eV; the twofold σ - π splitting between the group of $4t_{1u}$, $3e_g$, and $5a_{1g}$ levels and the $1t_{2u}$, $1t_{2g}$, $5t_{1u}$, $1t_{1g}$ group is evident.

V. ENERGY-BAND RESULTS

The valence and lowest conduction bands of MgO have been studied previously by Yamashita, using linear-combination-of-atomic-orbitals, (LCAO) methods^{38a} and the Green's-function approach, in the muffin-tin approximation.^{38b} A valence bandwidth of 9 eV was first obtained,^{38a} and this value was used by Fomichev *et al.*⁸ in an attempt to interpret x-ray absorption data. The more recent calculation gives a bandwidth of about 4 eV^{38b}; however, the direct band gap found is much too small. There is qualitative agreement between the Green's-function results and the present DVM calculation in the energy range where comparison is possible; however, significant quantitative differences are found. One of the important results of our work is to show that the use of an exchange parameter $\alpha = 0.82$ required to match the direct

gap deduced from optical data also yields a valence bandwidth of ~ 3.0 eV. This bandwidth, which is consistent with other recent calculations for ionic materials,^{17,18,39,40} is of great importance for further theoretical and experimental investigations, e.g., in estimating correlation effects and interpreting x-ray band tailing.

Therefore it is of considerable interest to see how modifications of the crystal potential, through choice of input atomic (ionic) configurations and exchange scaling, affect experimentally accessible gaps and bandwidths. The band structure of MgO has also been studied by Cohen and co-workers^{4,16} using the EPM fitted to the optical data. An interesting comparison of first-principles and empirical results for optical absorption is thus made possible.

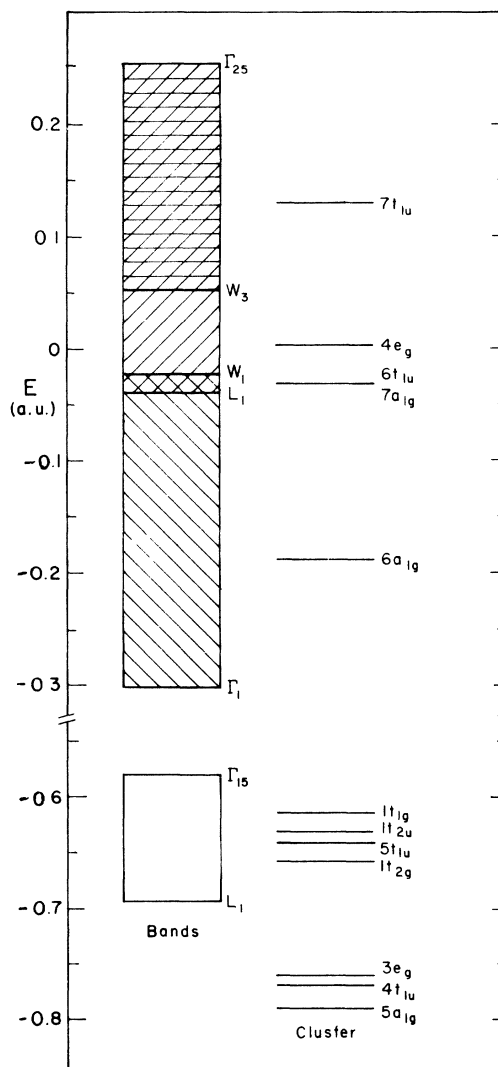


FIG. 2. Comparison of band and cluster energies. The three conduction bands have different shadings.

Basis functions for the variational calculations were constructed as Bloch sums of STO functions centered on metal and ligand sites. Considerable experimentation was done by varying the number and type of STO's to determine the effects of basis truncation on the band energies. The data presented here were generated using essentially the same STO set (Table I) used in the molecular-cluster calculations, and represent a reasonable compromise between accuracy and computational cost. Convergence of band energies as a function of the number of sampling points per cell was also investigated; approximately 1000 points per cell, chosen from superimposed atomiclike distributions,^{27,28} proved adequate for present purposes.

A typical set of energy bands for MgO are plotted along symmetry lines in Fig. 3; the corresponding Hamiltonian was generated from neutral atom configurations, with an exchange scaling parameter $\alpha = 0.82$. Aspherical (non-muffin-tin) contributions to the crystal potential are sizable, as shown in Fig. 4. The results are characterized by a narrow valence band mostly composed of oxygen $2p$ functions and, separated from the valence band by a wide energy gap, the broad "free-electron-like"

conduction bands. The conduction bands are shown up to an energy of 1.6 Ry. The computed energies are estimated to be converged within 0.005 Ry in the valence band and first conduction band, ~ 0.015 Ry in the next five conduction bands, and ~ 0.07 Ry in the highest three bands. A direct gap of 7.53 ± 0.07 eV at Γ is found, compared to the experimental value of 7.775 eV.⁵

In order to test the sensitivity of the bands to a scaling of the exchange factor, the energy values at the Γ and L symmetry points were recalculated for values of α ranging from 0.75 to 1.0. The resulting values of the energy gap and the valence bandwidth are plotted in Fig. 5. These important quantities are thus found to be quite sensitive to exchange scaling, changing by more than 30% over the stated range of α values. Very similar behavior was noted by Painter in his energy-band calculations for the highly ionic compound LiF.⁴⁰ While the energy gap and valence bandwidth scale in *opposite* fashion with increasing α , it should be noted that the four direct valence band-conduction band transitions (at Γ and L) plotted in Fig. 6 all scale in the same manner with α . In fact, the total change of each quantity is roughly 3 eV over the

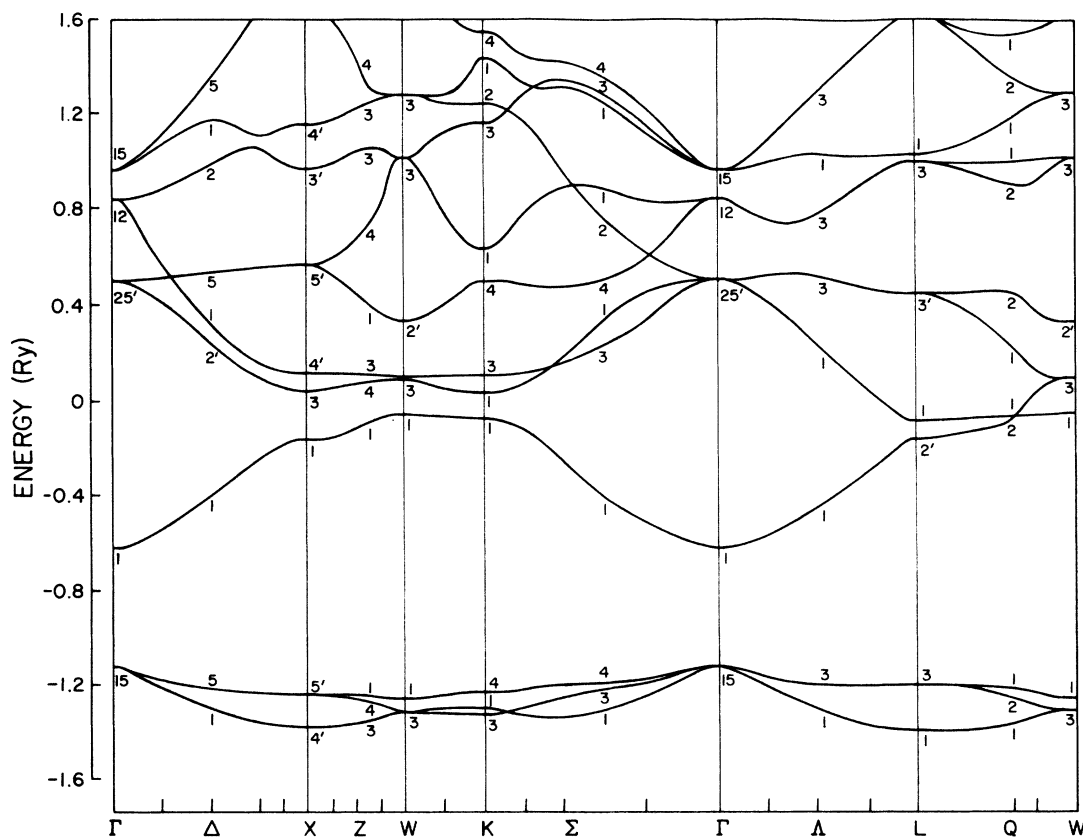


FIG. 3. Energy-band structure of MgO for $\alpha = 0.82$, with neutral atom configuration.

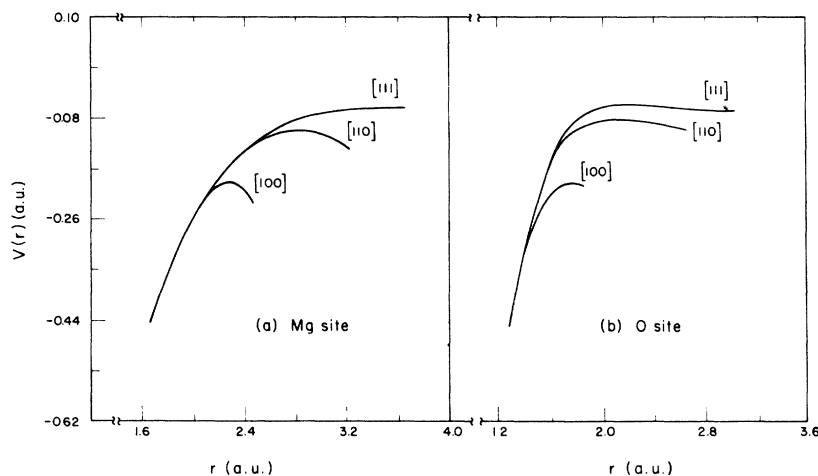


FIG. 4. Angular variation of crystal potential: (a) around the magnesium site, (b) around the oxygen site.

indicated range of α .

With this exchange sensitivity in mind, it is clearly also necessary to examine the effects of input atomic (ionic) configurations in an *ad hoc* non-SCF procedure. By comparing the results obtained with neutral atom Mg^0O^0 and ionic configurations Mg^+O^- and $\text{Mg}^{++}\text{O}^{--}$ as input, we expect to bracket the results to be obtained from an SCF calculation. The energy bands were recalculated along symmetry lines for each of the three potentials; in every case the resulting occupied eigenstates show well-defined $\text{Mg}^{++}\text{O}^{--}$ character, as expected in the conventional ionic model.³⁸ Significant changes in energies, aside from uniform shifts, are rather small, and thus help to justify use of the non-SCF results.

Changes occurring in several important band parameters with the three potentials (α fixed at 0.82) are shown in Fig. 7. Here $\Gamma_{15}-L_1$ is the valence bandwidth, $\Gamma_1-\Gamma_{15}$ is the fundamental gap,

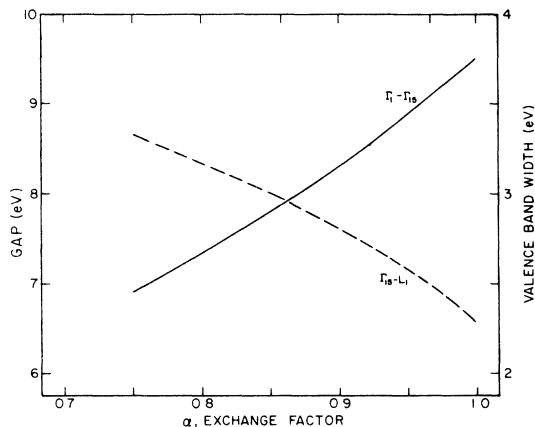


FIG. 5. Direct gap $\Gamma_1-\Gamma_{15}$ and valence bandwidth $\Gamma_{15}-L_1$ vs exchange parameter α .

$L_2'-L_3$ is a higher gap, and $\Gamma_{12}-\Gamma_{25}$ is the *d*-band splitting at Γ . We see that changing the assumed ionicity has a relatively small effect on important transition energies; e.g., the direct gap $\Gamma_1-\Gamma_{15}$ changes by about 15% over the entire range of potentials. This can be contrasted to changes of more than 30% when the exchange is scaled in the interval $0.75 \leq \alpha \leq 1.0$. Another interesting feature is the great stability of the *d*-band splitting at the Γ point. Further study of the results leads to the general conclusion that the bands generally undergo rigid upward shifts of several volts as the potential is changed from neutral atom to monovalent to divalent ionic.

We can gain some further understanding of these effects by examining the crystal wave functions. In Fig. 8 are plotted four Γ point crystal wave functions obtained in the DVM calculations. The $\Gamma_{1\nu}$ wave function, shown in Fig. 8(a), is a low-lying (~ -32 eV) bonding combination of magnesium 2s

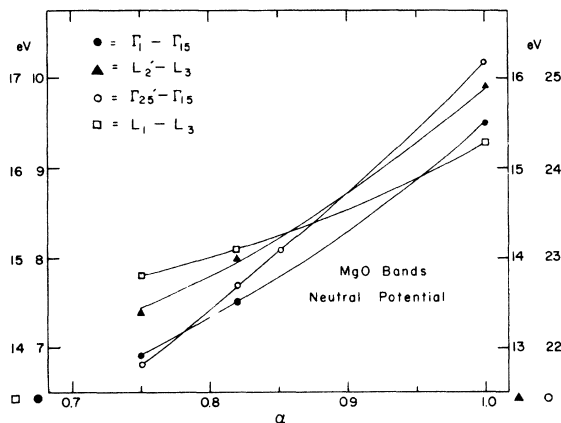


FIG. 6. Variation of important band transitions with exchange α .

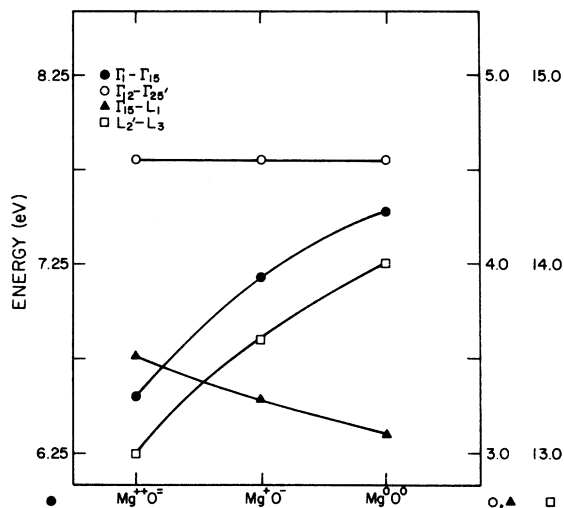


FIG. 7. Effect of assumed ionicity (input potential) on band transitions.

and mostly oxygen 2s. Figure 8(b) displays one representative state of the triply degenerate $2p$ -like occupied Γ_{15v} valence level; it is seen to be predominantly oxygen $2p$ with a slight magnesium $2p$ contribution. The first Γ conduction level is shown in Fig. 8(c), and is seen to be an almost equal mixture of Mg and O $3s$ functions. Finally, one state of the triply degenerate Γ_{25c} conduction level is shown in Fig. 8(d). This state consists of roughly equal parts of d functions on magnesium and oxygen.

Figures 8(b) and 8(c) offer a simple explanation for the sensitivity of the band gap and the valence bandwidth to exchange scaling. Since the first conduction band is s like and diffuse, it is affected by exchange in a different way than the p -like valence band. In the local exchange approximation, the exchange potential is proportional to the cube root of the electron charge density. The compact p -like valence functions have large amplitude in regions of high charge density whereas the Γ_{1c} function has less amplitude and is more spread out. Thus, increasing exchange has two effects on the valence band: the band is narrowed and shifted to lower energy. The first effect was seen in Fig. 5; the second effect is shown in Table III where some valence-band and first conduction-band energies are listed for various values of α . Increasing exchange also lowers the first conduction band, but not as much as the valence band; hence the band gap widens as α increases.

A. Comparison of Energy-Band and Cluster Results

In Fig. 2 we have compared valence and excited states from the band calculation and the MgO_6 clus-

ter calculation, using the same crystal Hamiltonian. We can restate our results for the cluster as follows: The cluster is found to have an energy gap and valence bandwidth which scale with α in the same manner as the energy bands. The valence-excited gap values of ~ 10 – 14 eV are considerably larger than the experimental gap, and the valence bandwidth is somewhat larger than that given by the energy-band calculation. Energy-band and cluster results are found to be almost identical for the (core) levels below the valence bands. Both models show the first excited states to be predominantly s like and of mixed Mg and O character.

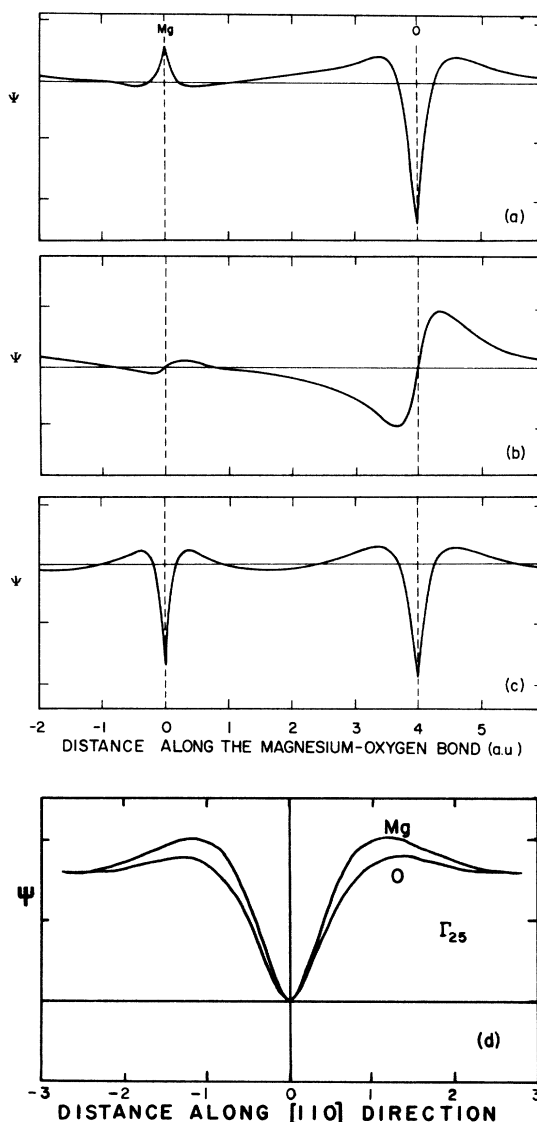


FIG. 8. Wave functions for valence and first conduction bands: (a) Γ_{15v} , (b) Γ_{15v} , (c) Γ_{1c} all along [100] bond axis, and (d) $3d$ -like Γ_{25c} state about both Mg and O sites.

TABLE III. Variation of several valence- and conduction-band energies with exchange parameter α (neutral atom configuration).

irrep	$\alpha = 0.75$ (eV)	$\alpha = 0.82$ (eV)	$\alpha = 1.0$ (eV)
Γ_{1c}	6.8	8.2	11.7
Γ_{15v}	13.7	15.8	21.2
$L_{2'c}$	0.8	2.2	5.7
L_{3v}	14.3	16.3	21.6

VI. CORE BINDING ENERGIES AND X-RAY DATA

A. Core Binding Energies

High resolution x-ray photoelectron spectra (XPS or ESCA) measuring electron binding energies for magnesium and oxygen K , L_I and $L_{II,III}$ shells are available for MgO.¹¹⁻¹⁴ Although difficulties in the determination of work functions and surface layer effects (including charging effects in insulators) are well known, a comparison with the calculated one-electron spectra is useful as a first approximation. This has been justified in the HF model by invoking Koopmans theorem; viz., that HF orbital energy eigenvalues give approximately the binding energies for the electrons. Orbital relaxation and multiplet hole interactions are neglected.

The experimental data are compared with one-electron energies (obtained with both MO and band schemes) in Table IV. Theoretical results are presented for neutral atom and divalent ionic input configurations; sizable changes due to exchange scaling are noted. It is evident that $\alpha = 0.82$ leads to a better match with valence levels. The Mg-1s binding energy is probably seriously underestimated because of the truncated STO basis used. As remarked previously, the absolute position of levels depends rather strongly upon assumed ionicity; e.g., in the $Mg^{++}O^{--}$ potential the Γ_{1v} (O 2s) level rises from 33 to 27 eV. With respect to XPS data, the divalent potentials are seen to be preferable;

TABLE IV. Comparison of MO and XPS binding energies (eV).

Experiment ^a	Mg ⁰ O ⁰	HFS-MO			
		$\alpha = 1$	$\alpha = 0.82$	Mg ⁺⁺ O ⁻⁻ : $\alpha = 0.82$	
Mg-1s	1305.3	$1a_{1g}$	1301	1269	1266
O-1s	532.2	$2a_{1g}$	567	547	539
Mg-2s	90.6	$3a_{1g}$	95	86	82
Mg-2p	51.7	$2t_{1u}$	63	53	49
O-2s	23.7	$4a_{1g}$	38	33	27
O-2p	6-10.5	$3t_{1u}, 2e_g$	22-27	17-22	10-15
		$5a_{1g}$			
		$4t_{1u}, \dots, 1t_{1g}$			

^aUnpublished data of G. K. Wertheim, MgO on Mg. Also see Refs. 11-13.

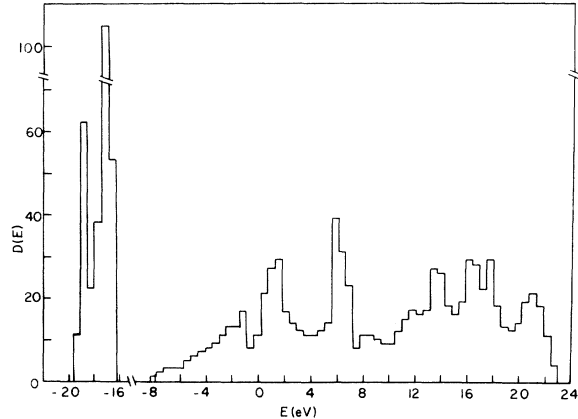


FIG. 9. Energy-band density of states $D(E)$.

however, more rigorous calculations are clearly desirable.

B. Densities of States

A general impression of features to be expected in both absorption and emission spectra can be obtained from the energy-band density of states (DOS) $D(E)$, which is shown in Fig. 9. The DOS, formed as a sum over individual band densities

$$d_j(E) = \frac{2}{(2\pi)^3} \int d^3k \delta[\mathcal{E}_j(\vec{k}) - E], \quad (8)$$

have been frequently used in the interpretation of photoemission and x-ray data. However, a detailed understanding requires the calculation of transition strength matrix elements, coupling initial and final states. An intermediate step not requiring extensive wave-function computations, but incorporating the \vec{k} selection rule (direct transitions) is followed here, making use of the interband densities of states

$$d_{ij}(E) = \frac{2}{(2\pi)^3} \int d^3k \delta[E_{ji}(\vec{k}) - E], \quad (9)$$

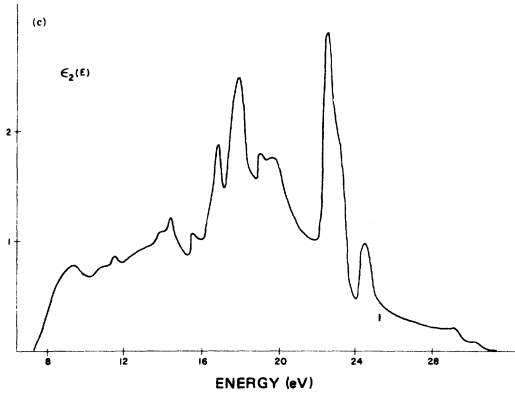
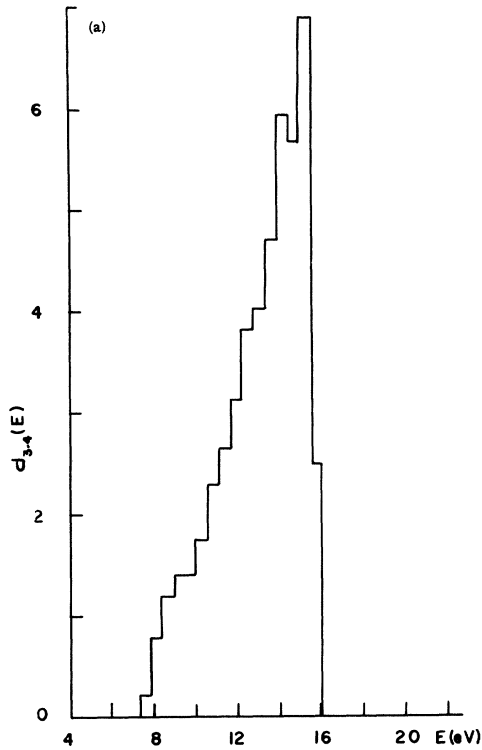
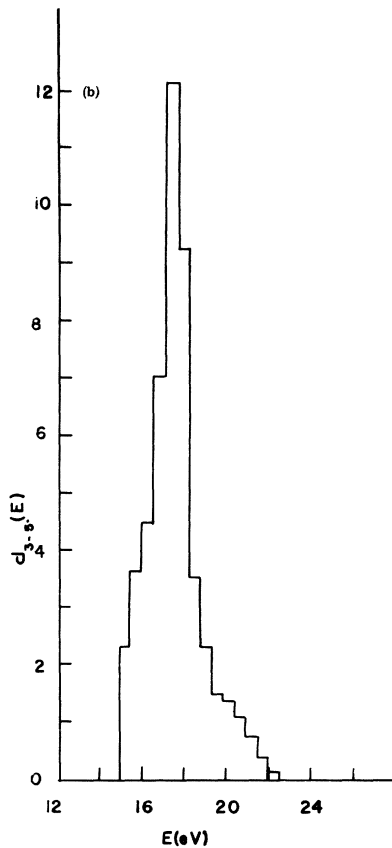


FIG. 10. Interband joint densities of states (a) d_{34} , (b) d_{35} , and (c) $\epsilon_2(E)$ obtained using oscillator strengths calculated between (1, 2, 3) valence bands and first five conduction bands.



where $E_{ji} = \mathcal{E}_j - \mathcal{E}_i$. In the "constant oscillator strength" approximation these quantities allow discussion of individual band-pair contributions to absorption and emission processes in both optical and x-ray energy ranges.

The DOS were calculated by straightforward procedures discussed in detail elsewhere.⁴¹ Briefly, the energy levels were determined at 45 inequivalent \vec{k} vectors in the Brillouin zone, and a least-squares fit to the energy bands was made, using symmetrized sums of plane waves. The optimum number of expansion functions was found to be about 25, representing a compromise between undesirable high-frequency ripple in the fit and minimum error on the data grid. The resulting rms errors in the energy-band fits were 0.003 a.u. in the valence bands, 0.01 a.u. in the first four conduction bands, and 0.02 in the five highest bands treated, and set a significance limit on the derived DOS. Thus, all DOS results were calculated with an energy resolution of 0.02 a.u. in the conventional histogram representation. The amplitudes were calculated by diophantine sampling; a precision of at least 3% was obtained using 8000 sample points. The results shown in Figs. 9 and 10 will be discussed in context with the x-ray and optical data.

C. X-Ray Data

In principle, x-ray emission spectra give at least a qualitative picture of the valence band, while absorption spectra provide a similar view of the conduction bands. By combining the two spectra

one hopes to determine band gaps, the width of the valence band, etc. The analysis is complicated by the presence of localized (excitonic) states, multiple ionization satellites, and such possible hybrids as "valence-electron configuration" states.^{42,43} Fortunately, much reliable data have become available and attempts have been made to correlate the band-structure calculations^{8,42,44} and MO models^{9,42,45} with the experimental results for various insulators. However, it is fair to say that interpretation of soft-x-ray data is still a developing art, compared to such established methods as optical reflectance and absorption analysis.

For MgO Fischer¹⁵ and Fomichev *et al.*⁸ have attempted an interpretation based on the band structure due to an ionic model of the crystal, while Dodd and Glenn⁹ have used an empirical MO approach. Analysis of x-ray data based on energy-band computations is the more traditional, while the MO scheme has recently been used by several authors⁴⁵ for covalently bonded materials. The importance of \vec{k} -dependent transition strengths for the understanding of x-ray intensities has been repeatedly emphasized⁴²; however, the required computation of matrix elements is rather tedious. The MO approach provides a simplification in that selection rules for allowed transitions are immediately determined from the known orbital symmetries. The allowed MO transition energies are expected to coincide with average values or peaks in the band excitation spectrum.

However, empirical models can lead to conflicting results; e.g., disagreement exists between the interpretation of the main $K\beta$ emission band of magnesium in MgO given by different workers. Fischer argues that $K\beta$ is a valence band (O- $2p$) to Mg- $1s$ "crossover" transition¹⁵; Dodd and Glenn would argue that $K\beta$ is a Mg- $3p \rightarrow 1s$ transition and that the bonding in MgO has a high degree of covalent character.⁹ They also attribute the splitting (2-3 eV) in the $K\beta$ line to the energy difference between σ^b and π^b (bonding) molecular orbitals constructed mainly from O- $2p$ levels. Their picture is based on empirical application of a qualitative MO energy-level model for octahedral complexes; no actual MO calculations were performed to justify this result.

The present HFS-MO calculations on the MgO₆ cluster resolve the $K\beta$ question in favor of Fischer's crossover model. However, many other features of the empirical MO model are compatible with our numerical results. One important result is the energy splitting found between the σ , π levels (together constituting the ligand "2p band"). We note that taking a weighted average of the energy levels in the two groups leads to a splitting of ~3 eV, depending slightly on the model potential employed. It is fairly clear that this splitting man-

ifests itself in three different parts of the MgO experimental spectra; the magnesium $K\beta$ and $L_{II,III}$ emission spectra and the oxygen K emission. All three spectra have about the same width, indicating a probable common origin in the oxygen- p valence band, and a splitting of 2-3 eV. We also note that our MO interpretation of the data allows for an immediate understanding of the lesser intensity of the low-energy peak. This follows from the fact that the electron population (DOS) of the σ levels is one-half that of the π levels. The strict application of MO electric dipole selection rules (O_h symmetry) is certainly not valid here since symmetry mixing of the levels in the crystal due to overlap with wave functions from atoms outside the cluster will occur. However, these selection rules can be used as a good first approximation in predicting the most important crossover transitions, as well as "one-center" terms.

Our results show that MgO comes out to be a divalent insulator, filling up energy levels to a Mg⁺⁺O⁻⁻ configuration, regardless of assumed ionicity used in constructing the Hamiltonian. The cross-over transition from the valence band MO's to the Mg- $1s$ level is allowed; however, the total transition energies found are only in fair agreement with experiment. The unoccupied $6a_{1g}$ MO state is separated by a gap of 10-13 eV from the valence band, and the valence bandwidth is ~5 eV. These results are compared with features of the energy-band DOS (Fig. 9) and with the results of optical reflectance measurements in Sec. VII.

The $K\beta'$ structure in Mg emission is also of some interest. Dodd and Glenn would argue that this structure, which is found to be about 14.5 eV below $K\beta$ in energy, is a satellite. Fischer claims that this structure is due to an O- $2s$ - Mg- $1s$ transition, and our computations again support this latter view. The ligand $2p$ valence MO's are separated from the $2s$ levels by 11-16 eV in all the calculations. Note that these crossover transitions are MO allowed since the ligand s states form t_{1u} , e_g , and a_{1g} symmetry orbitals, and thus O- t_{1u} - Mg- a_{1g} is a permitted electric dipole transition. A puzzling feature of the experimental results is the lack of a $K\beta'$ structure in the oxygen emission spectra in MgO. Such structure is dipole allowed and should be found about 14.5 eV below $K\beta$ in energy. The authors feel that such a peak does exist but has not been observed because the oscillator strength is too weak. The Mg $K\beta'$ structure is already weak and the matrix elements for such a transition are from an initial state t_{1u} MO primarily constructed from ligand s functions to a Mg- $1s$ final state. The corresponding oxygen transition, to the O- $1s$ level, takes place because of the Mg- $2p$ contribution to the initial state t_{1u} MO, but this contribution is weak, hence the predicted low intensity of the O- $K\beta'$ struc-

ture. These qualitative observations would be supported by a rigorous calculation of the transition probabilities.

Fomichev *et al.*⁸ identified structure in the Mg $L_{II,III}$ emission data with the $2p-2s$ splitting of Mg in MgO, and both MO and band calculations support this interpretation. This splitting occurs at about 38 eV, and our MO calculations show the splitting to be approximately 33 eV; the band calculations give the identical 33-eV results, with no other states in a comparable energy range. HF atomic calculations of Clementi³⁶ show a splitting in the atom of 40 eV. The XPS results (Table IV) give 90.6 eV for the Mg- $2s$ binding energy, and 51.7 eV for the Mg- $2p$ level, allowing a further experimental estimate of 39 eV for the splitting.

Now we may discuss further significant features of the band-structure results. Attempts have been made to correlate x-ray emission data with valence bandwidths and energy gaps, but these efforts are made quite difficult by many-body and instrumental effects. Estimates as high as 8.5 eV have been given for the valence bandwidth of MgO,⁸ but such figures are doubtless too high. Accurate energy-band calculations^{17,40} and optical reflectance experiments⁴ consistently show ionic solids to have much narrower valence bands than this. The valence bandwidth found in the present work is ~ 3 eV, in reasonable agreement with the EPM result.⁴ In addition, we note a pronounced twofold splitting in the valence-band DOS, shown in Fig. 9. This splitting is ~ 1.6 eV, while observed splitting in the x-ray emission data is 2–3 eV. In the cluster calculations, we saw that the HFS model (with α chosen approximately to match the band gap) reproduces the experimental splitting.

The initial rise in the conduction-band DOS follows the expected $E^{1/2}$ dependence. This leading edge structure is due almost entirely to the broad singly degenerate first conduction band, with the minor peak at 7.2 eV above the band edge due to the relatively flat region in this band after the cross-over at Q . For further discussion we label the bands, in ascending energy, as valence = (1, 2, 3), conduction = (4, 5, ...). The small gap between bands 4 and 5 which extends across most of the Brillouin zone is responsible for the minimum seen next. Now, one would expect the onset of x-ray absorption to the d bands to be found at an excitation energy around 18 eV, as there is considerable d character in the wave functions at, e.g., X_3 and W_3 . Indeed there is pronounced structure centered at 17.3 eV in $D(E)$, and this is found to come primarily from the relatively flat portions of bands 5 and 6. Prominent peaks in the conduction-band DOS are found at 17.3, 22.3, 29.6, 32.3, 32.8, and 36.8 eV above the top of the valence band. Fomichev and Zhukova¹⁰ identify d -band absorption

about 22 eV above the $L_{II,III}$ absorption edge, but this value now appears to be too high. The peak at 22.3 eV in $D(E)$ comes from the flat structure (principally along Δ) in bands 7 and 8. The 29.6-eV peak results from the ninth band which is flat through much of the zone (Δ , Z , Q , Λ), while the last three peaks are due to bands 10, 11, and 12, respectively.

It should also be mentioned that Fomichev *et al.*⁸ attribute the start of K x-ray absorption of oxygen in MgO to transitions to p -like conduction-band states about 4 eV above the bottom of the first (s -like) conduction band. A plot of the pertinent Γ_{1c} wave function [Fig. 8(c)] shows equal amounts of magnesium and oxygen s character; thus the O- $1s \rightarrow$ conduction-band transition is allowed, and of the crossover type. Also there are no p -like levels as close as 4 eV from the bottom of the conduction bands. It seems that the error in Fomichev's analysis lies in the attempt to match his x-ray data to an early LCAO band calculation of Yamashita^{38(a)} which gave a rather too large valence bandwidth of ~ 9 eV.

Finally, we note that inelastic Compton x-ray scattering measurements have been made⁴⁶ which appear to compare fairly well with an ionic model derived from the KKR band calculation.^{38(b)} More detailed studies of the momentum distribution arising from different points in the Brillouin zone have been undertaken, using wave functions obtained in the present work.

VII. OPTICAL PROPERTIES

Several experimental studies of the optical properties of MgO have been reported.¹⁻⁵ The reflectance data of Roessler and Walker extend up to 30 eV and have been used to extract the complex dielectric constant $\epsilon(\omega)$,³ and the exciton structure found at the low-energy edge has been the object of careful study.³⁻⁵ Exciton levels are observed to form just below the conduction-band minimum in compounds like the alkali halides⁴⁷ and MgO and thus mask the "true" single-particle (direct) absorption edge. For the purposes of this work, the result of primary interest is the interband absorption edge which results when the structure attributed to the exciton is subtracted off. By fitting the exciton structure with Lorentzian peaks and band edge with $E^{1/2}$ behavior, Whited and Walker were able to obtain a fundamental band gap of 7.775 eV.⁵ No mention is found in the literature of evidence for indirect (phonon-assisted) transitions, so remaining structure is presumed to be due to one-electron direct transitions, or plasma resonances. The main features of ϵ_2 observed are a sharp (exciton) peak at 7.7 eV, strong peaks at 10.8 and 13.2 eV, a weaker double peak at 16.8

and 17.3 eV, a "bump" at 20.5 eV, and weak broad structure over 23–24 eV.

A. MO Picture

The lowest predicted optical excitations are dipole allowed $5t_{1u}$, $4t_{1u} - 6a_{1g}$ transitions, occurring at 12.3 and 15.8 eV, using neutral atom potentials with $\alpha = 0.82$. As mentioned previously, the $6a_{1g}$ state corresponds to the center of gravity of the first conduction band, and indeed there is a strong peak in the experimental ϵ_2 data³ at 13.2 eV. These transitions are described most simply as charge transfer from O-2*p* to Mg-3*s*, although the upper level has a noticeable admixture of O-*s* character. Of course there is no evidence of the 7.7-eV exciton; more seriously, the experimental peak at 10.8 eV is not represented.

There are numerous allowed transitions from valence levels to the $6t_{1u}$, $7a_{1g}$, $4e_g$ levels, occurring between 16 and 21 eV. These can probably be related to the observed double-peak structure centered at 16.8 and 17.3 eV. These transitions are predominantly O-2*p* - 3*s* excitations. The bump observed at 20.5 eV is usually attributed to a bulk plasma resonance.³ Recalculation of transition energies, using divalent ionic configurations, led to shifts of ~ 0.8 eV toward lower energy.

B. Band Picture

The joint densities of states $d_{ij}(E)$ between valence band 3 and the first two conduction bands are shown in Fig. 10, together with the imaginary part of the dielectric function $\epsilon_2(E)$. The energy range up to ~ 30 eV is spanned. Optical studies of MgO by the EPM show 3-4 and 3-5 transitions to be most important.^{4,16} Thus it is very encouraging to note a considerable resemblance between the d_{34} and d_{35} first-principles results and the EPM data, which was obtained by fitting to experiment. However, the main peaks found in the present work occur ~ 1 eV higher than the EPM results. In addition to two main peaks, at 14.5 and 16.5 eV, $d_{34} + d_{35}$ DOS reveal a faint shoulder around 9–10 eV.

Since three valence bands are actually rather close together in energy the remaining d_{ij} contributions overlap considerably. Additional DOS peaks are noted at 18, 18.5, 19, and 19.5 eV corresponding to (1, 2, 3) - (5, 6) transitions. Valence - (6, 7) transitions involve states with *d* character on both metal and ligand sites, and show additional structure in the range 22–24 eV. We have calculated the interband oscillator strengths between valence bands (1, 2, 3) and the first five conduction bands throughout the Brillouin zone to determine the complete interband absorption measured by

$$\epsilon_2(E) = \frac{e^2 \hbar^2}{m} \sum_{i,j} \frac{1}{(2\pi)^3} \int d\mathbf{k}$$

$$\times f_{ij}(\mathbf{k}) \frac{\delta(E_{ji}(\mathbf{k}) - E)}{E_{ji}(\mathbf{k})}. \quad (10)$$

While marked variation of matrix elements with \mathbf{k} is found, as in our previous work on diamond,⁴¹ this is insufficient to reproduce the major peak at 10.8 eV. The theoretical ϵ_2 [Fig. 10(c)] shows weak peaks at 9.0 and 11.5 eV, as compared with a shoulder in the EPM model in the same energy range. Other important features include peaks centered around 14.0, 18.0, 19.0, 22.5, and 24.5 eV which appear 1–2 eV above the corresponding experimental peaks. The optical structure predicted by both the MO cluster and band models is listed in Table V along with the experimental ϵ_2 results. The MO model makes no prediction about either of the first two observed peaks, and the band model shows only weak structure near the second peak. A comparison of corresponding joint density of states results with the complete ϵ_2 calculation shows that use of \mathbf{k} -dependent oscillator strengths leads to a more rapid increase in absorption near the band edge, and produces peaks superimposed on the rising shoulder. However, the amplitude of these peaks falls well below the experimental ϵ_2 values. Omission of the 7.7-eV peak is not surprising, since this is well-established exciton structure, not contained in a one-electron model. But the inability of either model to predict the second (10.8 eV) peak is very serious. Our band computation was made with a value of α scaled to give approximate agreement with the experimental band gap. It is also possible to decrease the transition energies by decreasing α . Extrapolating from existing results, the authors estimate a value of $\alpha \sim 0.60$ would shift the d_{ij} data downward by ~ 2 eV and into agreement with the experimental third and fourth peaks (and give a band gap ~ 5.5 eV), but would still not give the second peak. Such a value of α is outside the recommended values and far from the optimum values found for atomic magnesium (0.73) and atomic oxygen (0.74).⁴⁸ Thus, we conclude that the lack of agreement with experiment is not simply a matter of scaling α but possibly reveals a basic limitation of the one-electron theory.

It is possible to use $\text{Mg}^{++}\text{O}^{--}$ atomic potentials to shift the important transition energies; it appears that we can gain at most 1 eV by doing this for $\alpha = 0.82$. Thus, a combination of scaling α and changing input atomic potentials could give the correct positions of the third and fourth reflectance peaks. But each alteration would give an incorrect band gap; it is not possible to obtain the third and fourth peaks and the band gap simultaneously, and no plausible set of changes will yield the first or second peaks. Similarly, the MO transition energies are reduced by less than 1 eV when the di-

TABLE V. Comparison of theory and experimental ϵ_2 optical data (eV).

Experiment ^a		EPM ^b	HFS-band ^c	HFS-MO ^c
7.7	exciton	7.76 gap	7.5 gap	...
10.8	peak	11.1 peak ^d	9.0 weak peak	...
13.2	peak	13.2 peak	11.5 weak peak	
16.8	peak	15.7 peak	14.0 peak	12.3
17.3	peak	16.2 peak	18.0 peak	
20.5	bump		19.0 peak	15.8, 15.9, 16.5
23-24	weak, broad		22.5 peak	
			24.5 peak	17.0, 17.2, 17.5
				19.8, 20.6

^aReference 3.^bReference 16.^cNeutral atom configurations, $\alpha = 0.82$.^dThis EPM peak is $\sim \frac{1}{3}$ of the experimental height, forming a rather broad shoulder.

valent configuration is employed.

Fong *et al.*¹⁶ assumed the first reflectance peak to be excitonic and constrained the second peak to be a one-electron transition in the EPM model. The EPM model associates transitions along Λ and at L with the 10.8-eV peak; interestingly, only a shoulder of height $\sim \frac{1}{3}$ that of the experimental peak is obtained by the gap-fitting procedure used. It is apparent that our first-principles results suffer the same fate even after the inclusion of oscillator strengths.

In summary, it is concluded that simple HFS one-electron band or MO theory, taken from a range of physically interesting input potentials, is not capable of explaining the first two reflectance peaks. The work of Roessler and Walker³ strongly supports the view that the first peak is a Γ point exciton. We in turn suggest the possibility that the second represents an L -point exciton. Since our calculation shows the $L_3 \rightarrow L_2$, M_0 critical-point transition to be about 14 eV, the predicted exciton binding energy of ~ 3 eV is probably too high. But our important transition energies (away from Γ) have been seen to be too high by roughly 1-2 eV so this binding could be lowered in the manner previously discussed.

The great resemblance between MgO and KBr optical spectra has been remarked previously.⁴ The existence of L -point excitons in alkali-halide and rare-gas crystals has been invoked by Phillips^{49,50} in explaining the optical data, based on band models very similar to that found for MgO. Measurements down to 77 °K on MgO⁴ do not reveal fine structure or temperature-dependent shift in the second peak, so the exciton hypothesis does not yet have a firm basis in experiment. A similar puzzle is found in the second reflectance peak of CdO,⁵¹ also having the rocksalt structure, indicating the importance of further work on this structure.

VIII. CONCLUSIONS

We have examined the predictions of the first-principles HFS model for optical absorption and soft-x-ray data in MgO, using both molecular-cluster and energy-band representations. Dependence of binding and excitation energies upon choice of potential was studied in the simplest one-electron scheme by varying assumed ionicity and exchange scaling parameter. A value of $\alpha = 0.82$ was found to approximately match the band gap; however, the band results do not reproduce the prominent 10.8-eV absorption peak. Similar results for the MO calculations suggest that this peak may be due to an intraband exciton, previously identified in rare-gas and alkali-halide crystals, rather than a one-electron transition. A valence bandwidth in reasonable accord with other recent calculations on insulators is obtained, but differences of 1-2 eV between experimental and theoretical splittings and positions of excitation energies suggest the need for including correlation effects in the excited state.

XPS photoemission and x-ray absorption and emission data can be correlated fairly well with both MO and energy-band results. These results serve to resolve several previous controversies over the nature of bonding in MgO and the origin of specific x-ray transitions. In particular, the $K\beta'$ structure in Mg emission is identified with the O-2s - Mg-1s crossover transition. The 2-3-eV splitting observed in x-ray emission is identified with a pronounced ~ 1.6 -eV twofold splitting found for the valence-band DOS, and with the 3-eV MO splitting. The absolute value of XPS binding energies is unknown, lacking a determination of charging effects and work function corrections. Similarly, theoretical \mathcal{E}_i binding energies depend rather sensitively on the model potential; however, the degree of agreement between theory and exper-

iment is encouraging. Valence-band structure visible in the XPS studies suggests further possibilities for extracting photoemission cross sections.

Both MO and energy-band results show the ground state of MgO to be essentially the simple divalent structure with ten electron atomic closed shells. Thus the HFS eigenfunctions obtained here should provide a good starting basis for treating correlation effects by methods developed for inert gas and alkali-halide crystals. A comparison of theoretical and experimental Compton profiles should provide an excellent further test of ground-state

properties, and work is in progress in this direction.

ACKNOWLEDGMENTS

We are indebted to Dr. G. K. Wertheim for making available his XPS data on MgO, and to Professor A. J. Freeman and Professor K. H. Johnson for stimulating discussions. We thank A. R. Lubinsky for assistance in the optical calculations. Computations were performed at the Vogelback Computing Center of Northwestern University.

[†]Part of this work represents a thesis submitted by P. F. Walch to the Dept. of Physics, Northwestern University, in partial fulfillment of the requirements for the Ph.D. degree. Research supported in part by the Air Force Office of Scientific Research Grant No. 71-2012, and by the Advanced Research Projects Agency through the Northwestern University Materials Research Center.

*Alfred P. Sloan Research Fellow.

¹G. H. Reiling and E. B. Hensley, *Phys. Rev.* **112**, 1106 (1958).

²M. W. Williams and E. T. Arakawa, *J. Appl. Phys.* **38**, 5272 (1967).

³D. M. Roessler and W. C. Walker, *Phys. Rev. Lett.* **17**, 319 (1966); *Phys. Rev.* **159**, 733 (1967); *J. Opt. Soc. Am.* **57**, 835 (1967).

⁴M. L. Cohen, P. J. Lin, D. M. Roessler, and W. C. Walker, *Phys. Rev.* **155**, 992 (1967).

⁵R. C. Whited and W. C. Walker, *Phys. Rev. Lett.* **22**, 1428 (1969).

⁶D. W. Fischer and W. L. Baun, *Spectrochim. Acta* **21**, 443 (1965).

⁷H. U. Chun and D. Hendel, *Z. Naturforsch. A* **22**, 1401 (1967).

⁸V. A. Fomichev, T. M. Zimkina, and I. I. Zhukova, *Fiz. Tverd. Tela* **10**, 3073 (1969) [*Sov. Phys.-Solid State* **10**, 2421 (1969)].

⁹C. G. Dodd and G. L. Glenn, *J. Appl. Phys.* **39**, 5377 (1968).

¹⁰V. A. Fomichev and I. I. Zhukova, *Fiz. Tverd. Tela* **10**, 3753 (1968) [*Sov. Phys.-Solid State* **10**, 2992 (1969)].

¹¹A. Fahlman, K. Hamrin, R. Nordberg, C. Nordling, and K. Siegbahn, *Phys. Rev. Lett.* **14**, 127 (1965); K. Siegbahn, C. Nordling, A. Fahlman, R. Nordberg, K. Hamrin, J. Hedman, G. Johannson, T. Bergmark, S. Karlsson, I. Lindgren, and B. Lindberg, *ESCA, Atomic, Molecular and Solid-State Structure Studied by Means of Electron Spectroscopy* (Almqvist and Wiksells, Stockholm, 1967), and references contained therein.

¹²S. Hagstrom and S. E. Karlsson, *Ark. Fys.* **26**, 451 (1964).

¹³R. Nordberg, K. Hamrin, A. Fahlman, C. Nordling, and K. Siegbahn, *Z. Phys.* **192**, 462 (1966).

¹⁴G. K. Wertheim (unpublished data).

¹⁵D. W. Fischer, *Adv. X-Ray Anal.* **13**, 159 (1970).

¹⁶C. Y. Fong, W. Saslow, and M. L. Cohen, *Phys. Rev.* **168**, 992 (1968).

¹⁷P. D. DeCicco, *Phys. Rev.* **153**, 931 (1967).

¹⁸L. F. Mattheiss, *Phys. Rev. B* **5**, 290 (1972); *Phys. Rev. B* **5**, 306 (1972).

¹⁹A. B. Kunz, *Phys. Status Solidi* **36**, 301 (1969).

²⁰N. O. Lipari, *Phys. Rev. B* **6**, 4071 (1971), and references therein.

²¹J. C. Slater, *Phys. Rev.* **81**, 385 (1951).

²²W. Kohn and L. J. Sham, *Phys. Rev.* **140**, A1133 (1965).

²³R. Gaspar, *Acta Phys. Acad. Sci. Hung.* **3**, 263 (1954).

²⁴I. Lindgren, *Ark. Fys.* **31**, 59 (1965); *Phys. Lett.* **19**, 382 (1965).

²⁵J. C. Slater [*Quantum Theory of Molecules and Solids* (McGraw-Hill, New York, 1963), Vol. 1] provides a good

exposition of the HF and HFS models.

²⁶J. C. Slater and K. H. Johnson, *Phys. Rev. B* **5**, 844 (1972), and references therein.

²⁷T. Parameswaran and D. E. Ellis, *Int. J. Quantum Chem. Symp.* **5**, 443 (1971); T. Parameswaran and D. E. Ellis, *J. Chem. Phys.* **58**, 2088 (1973).

²⁸G. S. Painter and D. E. Ellis, *Phys. Rev. B* **1**, 4747 (1970); D. E. Ellis and G. S. Painter, *Phys. Rev. B* **2**, 2887 (1970).

²⁹A. A. Frost, *J. Chem. Phys.* **10**, 240 (1942); A. A. Frost, R. E. Kellogg and E. C. Curtis, *Rev. Mod. Phys.* **32**, 313 (1960).

³⁰C. M. Carlson, *J. Chem. Phys.* **47**, 862 (1967); D. K. Harris and C. M. Carlson, *J. Chem. Phys.* **51**, 5458 (1969).

³¹D. H. Bell and L. M. Delves, *J. Comput. Phys.* **3**, 453 (1969).

³²(a) D. E. Ellis and G. S. Painter, in *Computational Methods in Band Theory*, edited by P. M. Marcus, J. F. Janak, and A. R. Williams (Plenum, New York, 1971), p. 271; (b) G. S. Painter and D. E. Ellis, in Ref. 32a, p. 276.

³³D. E. Ellis, *Int. J. Quantum Chem. Symp.* **2**, 35 (1968); G. S. Painter and D. E. Ellis, *Int. J. Quantum Chem. Symp.* **3**, 801 (1970).

³⁴G. S. Painter, *Phys. Rev. B* **7**, 3520 (1973).

³⁵R. W. G. Wyckoff, *Crystal Structures*, 2nd ed. (Interscience, New York, 1963), Vol. 1, p. 88.

³⁶E. Clementi, *IBM J. Res. Dev. Suppl.* **9**, 2 (1965).

³⁷Further details may be found in P. F. Walch, thesis (Northwestern University, 1972) (unpublished).

³⁸(a) J. Yamashita, *Phys. Rev.* **111**, 733 (1958); (b) J. Yamashita and S. Asano, *J. Phys. Soc. Jap.* **28**, 1143 (1970).

³⁹R. C. Chaney, E. E. Lafon, and C. C. Lin, *Phys. Rev. B* **4**, 2734 (1971).

⁴⁰G. S. Painter, *Int. J. Quantum Chem. Symp.* **5**, 501 (1971).

⁴¹A. R. Lubinsky, D. E. Ellis, and G. S. Painter, *Phys. Rev. B* **6**, 3950 (1972).

⁴²D. J. Nagel, *Adv. X-Ray Anal.* **13**, 182 (1970), and references therein.

⁴³L. G. Parrott, *Rev. Mod. Phys.* **31**, 616 (1959).

⁴⁴D. W. Fischer, *J. Appl. Phys.* **41**, 3922 (1970).

⁴⁵D. W. Fischer, *J. Appl. Phys.* **41**, 3561 (1970), and references contained therein.

⁴⁶R. J. Weiss, *Philos. Mag.* **21**, 1169 (1970); S. Togawa, O.

Inkinen, and S. Manninen, *J. Phys. Soc. Jap.* **30**, 1132 (1971).

⁴⁷J. E. Eby, K. J. Teegarden, and D. B. Dutton, *Phys. Rev.* **116**, 1099 (1959).

⁴⁸K. Schwarz, *Phys. Rev. B* **5**, 2466 (1972).

⁴⁹J. C. Phillips, in *Solid State Physics*, edited by F. Seitz and D. Turnbull (Academic, New York, 1966), Vol. 18; D. L. Greenaway and G. Harbeke, *Optical Properties and Band Structures of Semiconductors* (Pergamon, Oxford, England, 1968).

⁵⁰J. C. Phillips, in *The Optical Properties of Solids*, edited by J. Tauc (Academic, New York, 1966), p. 155.

⁵¹J. L. Freeouf, *Phys. Rev. B* **7**, 3810 (1973), and private communication.